Materials Today Communications 30 (2022) 103045

Contents lists available at ScienceDirect

Materials Today Communications

journal homepage: www.elsevier.com/locate/mtcomm

Molecular dynamics study of SO_2 gas adsorption in two Y Zeolites: Effects of external fields

Yalda Sabahi [a], Mohammad Razmkhah [b,*], Fatemeh Moosavi [a,*]

[a] Department of Chemistry, Faculty of Science, Ferdowsi University of Mashhad, Mashhad 9177948974, Iran
[b] Department of Chemical Engineering, Faculty of Engineering, Ferdowsi University of Mashhad, Mashhad 9177948944, Iran

ARTICLE INFO

Keywords:
Molecular dynamics simulation
Y zeolite
Sulfur dioxide
Adsorption energy
External field
Potential of mean force

ABSTRACT

The present study evaluated the interaction energy values of adsorbed gas molecules by porous nanomaterials and the effects of external magnetic and electric fields on SO_2 adsorption in two Y zeolites with Si/Al ratios of ∞ and 3.0 using molecular dynamics simulation. Two types of external (electric and magnetic) fields were applied along the z-axis, and increased SO_2 adsorption was observed only in silica zeolite with the electric field. The magnetic field had no significant effect on SO_2 adsorption. Noticeably, the external electric field increased the SO_2 adsorption by the target materials, and the adsorption capacity was observed to improve compared to the magnetic field. The results of the radial distribution function and the potential of mean force disclose that SO_2-Y zeolite affinity enhanced and the adsorption energy is responsible for this observation. Since applying an electric field intensifies the structural ordering of SO_2 gas, it may also be involved in the improvement of the adsorption capacity. Moreover, the comparison of the two Y zeolites indicated that the zeolite with a lower Si/Al ratio validated a higher affinity toward SO_2, thereby resulting in a more significant adsorption saturation capacity.

1. Introduction

Fossil fuels have the most significant contribution to energy generation through 80% of the world's total energy [1]. The flue gas generated by car exhaust contains ppm levels of acidic gases, including CO_2, SO_2, and NO_2, with SO_2 considered a corrosive gas. Despite the significant growth in industrial processes, the control of SO_2 emissions remains challenging [2–4]. Acid rains, photochemical smog, and some of lung irritations are quite a few problems caused by acid gas.

Absorption, adsorption, and membrane separation are among the most promising techniques applied in industries to filter SO_2. In terms of industrial usability, the SO_2 removal process should be simple, single-step, and cost-efficient [5,6]. The adsorption of SO_2 in nanoporous solids is an alternative technique attracting great attention [7].

Among lots of adsorbents used in the industry, zeolites are considered as safe, effective, and affordable materials to capture and storage SO_2 [8–10]. One of the most common type of zeolites is Y zeolite; ordered pore structure, large surface area, and large mass transfer coefficient are the key advantages of this adsorbent [11,12]. Marcu and Sandulescu [13] performed desulfurization using Y zeolite at specific temperature and concentration ranges, reporting that the sorbent had a high adsorption capacity. Moreover, Lee et al. [14] investigated the desulfurization of a solution with a bimetal-exchanged mesoporous Y zeolite, observing its high capacity and selectivity for sulfur separation. He et al. [15] also investigated the adsorption of dibenzyl disulfide using Y zeolites reporting that the adsorption efficiency enhanced rapidly with the increased metal dosage in the zeolite. In another study, Khalil et al. [16] denoted the selective capture of phenol by Y zeolites. Cerutti et al. [17] also assessed desulfurization from gasoline using copper-exchanged Y zeolites.

Acidic gases may degrade multiple adsorbents by poisoning the structure and blocking the channels due to the strong binding between the adsorbent and adsorbate. Therefore, selecting the optimal adsorbent is paramount. On the other hand, the insertion of metals with magnetic properties [18] increases the performance of the adsorbent. In such a case, an external static magnetic/electric field is applied to investigate their effects on gas adsorption rather than changing the chemical structure of the adsorbent. It is well-established that external fields

Abbreviations: ADF, Angle Distribution Function; DFT, Density Functional Theory; LJ, Lennard-Jones; MDS, Molecular Dynamics Simulation; Mn-Gr, Mn-doped Graphene; MSD, Mean Square Displacement; P-Gr, Phosphorus-doped Graphene; PMF, Potential of Mean Force; RDF, Radial Distribution Function; vdW, van der Waals.

* Corresponding authors.
E-mail addresses: mohammad.razmkhah@mail.um.ac.ir (M. Razmkhah), moosavibaigi@um.ac.ir (F. Moosavi).

https://doi.org/10.1016/j.mtcomm.2021.103045
Received 7 April 2021; Received in revised form 23 November 2021; Accepted 26 November 2021
Available online 29 November 2021
2352-4928/© 2021 Elsevier Ltd. All rights reserved.

affect numerous adsorption properties [19–21]. Razmkhah et al. [22] investigated the effects of magnetic and electric fields on CO_2 adsorption on graphene oxide framework observing a significant increase in CO_2 adsorption in the presence of a strong external electric field; however, magnetization did not play a key role in adsorption capacity. In another study, Sun et al. [23] evaluated CO_2 capture on MoS_2 monolayers controlled by an external electric field by density functional theory (DFT). According to the obtained results, CO_2 strongly interacted with MoS_2 monolayers in the presence of electric field. In addition, Zhang et al. [24] considered the electric field-controlled capture of phosgene molecules on Mn-doped graphene (Mn-Gr) sheets through first-principle simulations and their findings indicated that the adsorption energy of phosgene on Mn-Gr was significantly improved by the electric field. Qin et al. [25] assessed controllable CO_2 adsorption on a C_2N monolayer using DFT computation observing that CO_2 adsorption increased by applying an external electric field. In addition, Esrafili [26] explored the effect of an electric field on CO_2 capture by phosphorus-doped graphene (P-Gr) using DFT. The obtained results indicated that at a specific electric field, CO_2 is strongly adsorbed on P-Gr. In another research, Ma et al. [27] used sodium alginate/graphene/L-cysteine (SA/GR/L-Cys) beads for the adsorption of pollutants denoting that using a rotating magnetic field positively influenced adsorption. The aforementioned studies show that applying an external field may play a crucial role in adsorption capacity.

The present study aimed to evaluate the adsorption of SO_2 gas in the cages of two Y zeolites using molecular dynamics simulation (MDS). Since SO_2 is a polar molecule, its adsorption may be affected by an external field; consequently, the main objectives of the current research could be summarized as follows:

- Assessing the effects of external electric and magnetic fields on adsorption capacity and the structural behavior of SO_2 inside the target Y zeolites.
- Evaluating the effects of aluminum and cation on the adsorption capacity of the zeolites.

To the best of our knowledge, the effects of an external field on the adsorption and removal of SO_2 by zeolites have not been studied from a molecular perspective so far.

2. Simulation details

The primary structure of the cubic unit cell ($Fd\bar{3}m$) of the silica Y zeolite with $Si_{192}O_{384}$ formula and unit cell of $a = 24.345$ Å was created based on the crystallographic information file obtained from the database of zeolite structures [28]. For NaY, the chemical composition $Si_{192-x}Al_xNa_xO_{384}$ was considered with $x = 48$ to reproduce the Si/Al ratio of 3.0. The framework was built in accordance with Löwenstein's Al-O-Al avoidance rule [29]. The second stage involved the distribution of Na extra framework cations among various crystallographic sites of the zeolite as described by Plant et al. [30].

According to the literature [12,31–33], if the adsorbate is tightly fitted to the adsorbent, the framework flexibility is essential. This is because lattice vibration removal leads to the overestimation of the energy barriers for transferring the guest molecules within the crystal. In contrast, in the case that the guest molecule has a smaller kinetic diameter than the zeolite pore openings, a fixed adsorbent framework does not have a significant effect on the guest molecule dynamics. In addition, the frameworks that exhibit remarkable breathing should be considered flexible; such effect has not been observed in Y zeolites with relatively wide channels and corrugated walls. Considering that the kinetic diameter of SO_2 is 3.6 Å, the fixation of the zeolite framework does not have a remarkable impact on the magnitude of the diffusivity trend [31]. The 12-member windows of the Y zeolite had a diameter of 7.4 Å [34], and the SO_2 molecule was considered rigid with a bond length of 1.431 Å, and the bond angle of O-S-O was equal to 119° [35]. The Lennard-Jones (LJ) potential was also used for the van der Waals (vdW) pair interactions; the partial atomic charges and LJ parameters reported for the SO_2 gas and Y zeolite were applied [36–39]. The LJ parameters between various atom types were generated from the Lorentz-Berthelot mixing rules, $\varepsilon_{ij} = \sqrt{\varepsilon_{ii}\varepsilon_{jj}}$ and $\sigma_{ij} = \frac{1}{2}(\sigma_{ii} + \sigma_{jj})$ [10,37].

All simulations were performed using DL_POLY package version 2.17 [40,41] on a Linux workstation. One unit cell of each Y zeolite was used as the simulation box as the size effect could not be recognized for the system of concern [20]. Several studies have investigated the effect of the simulation cell size on the adsorption of guest molecules, indicating that the size effect is negligible [11,42]. For instance, Zheng et al. [43] selected two sizes of unit cell ($1 \times 1 \times 1$ and $2 \times 2 \times 2$ of Y zeolite) to adsorb guest molecules and observed similar results for the adsorption energies.

In the present study, periodic boundary conditions were also applied and the simulations were carried out at a constant temperature (300 K) by rescaling the velocities to control the desired temperature. The initial structure was equilibrated for 2 ns and MDS runs for data production were continued for 1000 ps. The timestep in all the simulations was set at 1 fs and the cut-off radius was 12 Å. Moreover, equations of motion were integrated using the leapfrog algorithm [44]. The Ewald summation method was applied to compute long-range electrostatic interactions. Orthorhombic three-dimensional periodic boundary conditions were selected with a simulation box of 75 Å in the z-direction and x-y plane of 24.345×24.345 Å^2; see Fig. 1.

To calculate the adsorption isotherm, the gas molecules were placed in the space outside the zeolite and initially directed by applying

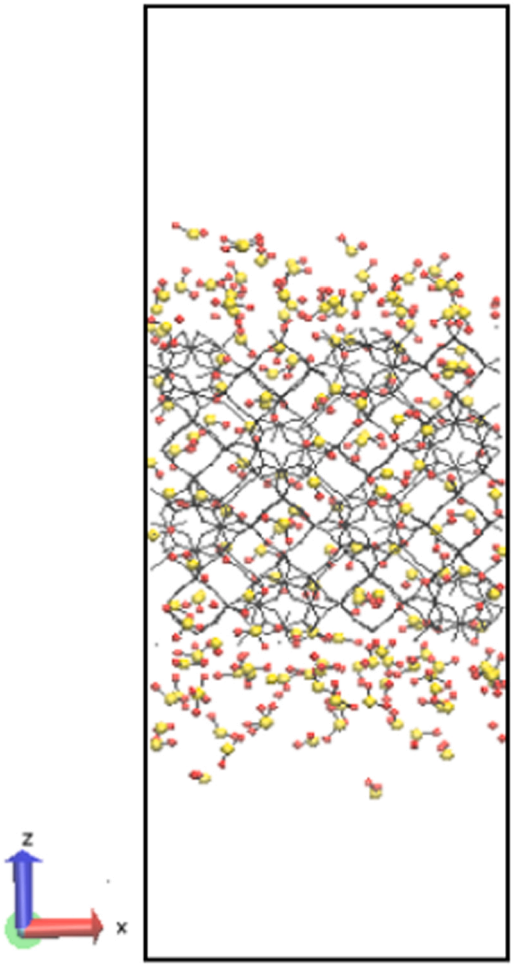

Fig. 1. A snapshot of simulation box.

pressure into the pores of the Y zeolite. Following that and at each time interval, a configuration was selected with various loadings of the gas molecules inside the pores. The main simulations were initiated with the desired number of SO_2 molecules inside the pores. Throughout the process, some of the SO_2 molecules spontaneously filled the outer space of the zeolite. At the end of the simulation, only the gas molecules inside the zeolite that were at least 0.5 Å away from the zeolite inner surface were considered to quantify the adsorption isotherm. Finally, the loading capacity was calculated based the number of the adsorbed gas molecules and the adsorbent mass. In addition, the number of the molecules that were not adsorbed in each simulation was used to calculate the gas pressure using the ideal gas equation of state. Following that, simulation was repeated with the same procedure to determine the gas/zeolite binding.

The interatomic potential of mean force (PMF), $w_{ij}(r)$, offers the interaction energy of the SO_2/zeolite as a function of the separation distance between the two species i and j [45]:

$$w_{ij}(r) = -RT \ln g_{ij}(r) \tag{1}$$

where R is the gas universal constant, T shows the simulation temperature, and $g_{ij}(r)$ is the pair radial distribution function (RDF). Analyzing the atomic correlation based on RDF indicated the probability of finding a particle at a certain distance to another particle [46]:

$$g_{ij}(r) = \frac{V}{N}\frac{N_j(r)}{4\pi r^2 \Delta r} \tag{2}$$

where i and j represent the two species, V is the volume of the system, N shows the total number of all the species, and $N_j(r)$ is the number of the j species in the spherical shell with Δr width around the i species.

To obtain the orientation of the SO_2 gas inside the Y zeolite, a mixed angle/radial distribution function was computed [47]. To perform this evaluation, the phase space was split into a linear mesh; after that, the RDF value was collected into the linear RDF histogram and angle distribution function (ADF) values were added to the linear ADF histogram; as a result, the two-dimensional meshes were connected and linked. The ADF is an angle distribution of the particles relative to a specified direction [48]. In our study, the angle between the z-axis and a vector passing through the O-S-O angle bisector was considered as α_{SO_2}. Fig. 2 shows the α_{SO_2} angle for the ADF analysis. As can be seen, the z-axis is a vector that is normal to the surface of the adsorbent.

According to Shi and Wang [49], an external electric field that is known as a weak electric field, was applied in the present study along the z-direction, as follows:

$$F = q.E,\ E(E_x,\ E_y,\ E_z) \tag{3}$$

where E represents the electric field vector (V/m), and q shows the atomic charge (C). To address this objective, the electric field of 10 V/m was applied along the z-axis; it is worth mentioning that just only the physical effect is under consideration and this magnitude of electric force is not enough to compensate for the chemical bonds, leading to any chemical effect. In addition, an external magnetic field was applied in the z-direction [50] and calculated using the following equation:

$$F = q.(v \times H),\ H(H_x,\ H_y,\ H_z),\ \text{and}\ v(v_x,\ v_y,\ v_z) \tag{4}$$

where H shows the magnetic field vector (T) and v is the velocity vector (m/s). Here, a magnetic field of one tesla (1 T) along the z-axis was applied.

3. Results and discussion

To ensure the sufficiency of the simulation time, the simulation continued for another 3 ns. Fig. 3 depicts the silica Y zeolite RDF in the absence of an external field in both simulations.

In addition to the similarity of the findings, no significant change could be observed in the number of the adsorbed gas molecules. Therefore, the simulation time of 3 ns was selected to analyze the obtained results. We also explored the adsorption of SO_2 into the two Y zeolite systems with the Si/Al ratio of ∞ and 3.0 in the presence and absence of the external electric and magnetic fields. To investigate the effects of the magnetic and electric fields on adsorption, a series of simulations were carried out. Initially, the adsorption isotherms were reported, followed by a structural analysis of the zeolites.

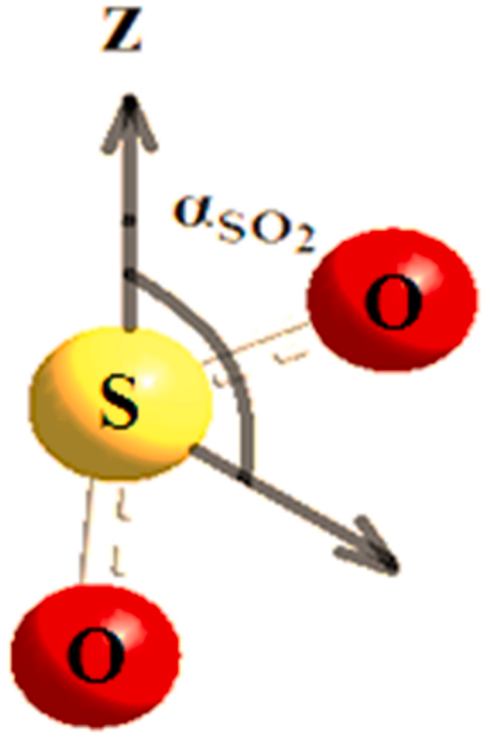

Fig. 2. Angle between z-axis and vector passing through O-S-O angle bisector, α_{SO_2}.

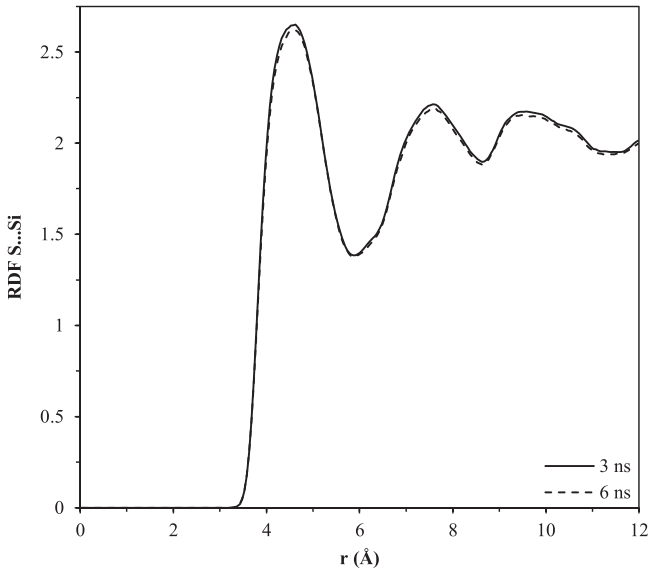

Fig. 3. RDF of S atom of SO_2 gas and Si atom of silica Y zeolite after 3 and 6 ns of simulation times.

3.1. Adsorption isotherm

For several decades, acidic gas adsorption by porous materials has been extensively studied to explore the essential behavior of gas adsorption from a molecular perspective. Furthermore, some models have been introduced to describe gas adsorption isotherms, which generally include theoretical, semi-empirical, and empirical models. Such examples are the Langmuir, Freundlich, Brunauer-Emmett-Teller (BET), and Guggenheim-Anderson-de Boer (GAB) isotherms [51,52]. Regarding certain thermodynamic assumptions, adsorption equilibrium could provide significant data on surface properties and gas adsorption mechanisms at a fixed temperature. In the present study, the adsorption isotherm of SO_2 in silica and NaY (Si/Al=3.0) at the temperature of 300 K was computed using MDS.

Fig. 4a illustrates the predicted isotherms for SO_2 in the silica Y zeolite in the presence of the electric field (E) and magnetic field (M), as well as the absence of each external field (No). As is shown, SO_2 adsorption significantly changes in the presence of the electric field. The electric field substantially increased not only the adsorption capacity but also the sensitivity of the adsorption to the pressure. On the other hand, the magnetic field decreased the sensitivity of the adsorbent to the pressure at $P < 4$ MPa, while increasing the adsorption capacity of the silica Y zeolite at a high pressure ($P > 4$ MPa).

Fig. 4b depicts the adsorption isotherms of SO_2 in the NaY zeolite in the presence and absence of the external fields. As can be seen, the electric field increased the adsorption capacity of the NaY zeolite at higher pressures than 6.6 MPa while the electric field significantly decreased the adsorption sensitivity at the pressure of $P < 6.6$ MPa. However, the electric field increased the adsorption capacity at the pressure of $P > 6.6$ MPa. Compared to the silica Y zeolite, a slight increase was observed in the adsorption capacity at the pressure of $P > 4$ MPa by using magnetization in the system despite the reduction in the adsorption sensitivity at the pressure of $P < 4$ MPa.

According to the obtained results, the polar characteristics of the SO_2 gas with an electric dipole moment of 2.0269 D, which was computed at B3LYP/6–311 + +G(d, p) level of theory, was the main reason for the significant difference in this regard; this is consistent with previous theoretical and experimental findings [53]. By applying an external electric field, the polar molecules aligned in the direction of the external field and dipole moment of SO_2 changed to 2.0321 D, thereby, creating extra available space for adsorption in the Y zeolite. Since this gas is diamagnetic [53,54], the effect of the external magnetic field on its adsorption is not significant; however, the electric field applied on the two Y zeolites is more effective compared to the magnetic field. The observed variation was associated with the affinity of SO_2/adsorbent and the phase change due to the adsorbed gas which explains the gas adsorption affinity based on PMF (Section 3.4).

3.2. Langmuir isotherm model

The adsorption isotherm for each zeolite system was fitted to the Langmuir model as described by Yang et al. [55].

$$C = \frac{C_{sat} bP}{1 + bP} \tag{5}$$

where C and C_{sat} are the loading capacity and saturation capacity, respectively, b represents the adsorption coefficient, and P is the gas pressure. The evaluated Langmuir parameters are summarized in Table 1.

According to the information in Table 1, applying an external field increased the saturation capacity (C_{sat}) not only in the silica Y zeolite but also in the NaY zeolite. Additionally, the replacement of some Si atoms in silica with Al and Na ions led to a more significant adsorption capacity. Therefore, it could be inferred that the Langmuir model decreased the adsorption coefficient in the presence of the external field. Furthermore, the adsorption coefficient was the lowest in the presence of the external electric field in the NaY zeolite. The goodness of fit was also acceptable and it could be observed that the saturation capacity of Si/Al= 3.0 (NaY) was more substantial compared to silica. The gas/adsorbent affinity may shed light on these simulation results.

Table 1
Langmuir isotherm parameters for studied gas in each zeolite.

System	C_{sat} (mmol/g)	b (MPa)	*R-squared*
No-silica	7.48	4.18	0.98
M-silica	8.37	1.37	0.99
E-silica	9.22	3.23	0.99
No-NaY	8.09	2.56	0.99
M-NaY	8.38	1.85	0.99
E-NaY	9.30	0.68	0.99

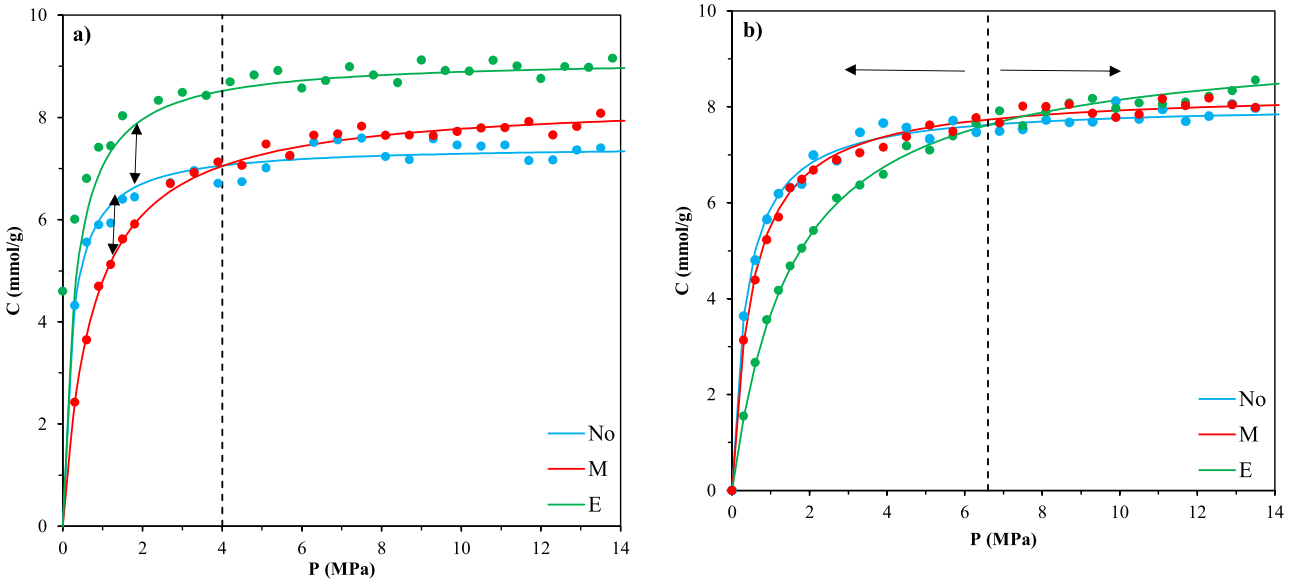

Fig. 4. Adsorption isotherm of SO_2 before (no Field) and after applying external fields in direction of z-axis at 300 K in a) silica Y and b) NaY. Dots are results of MD and lines show fitting data. See also Fig. S1 and Fig. S2 of Supplementary Materials.

3.3. Radial distribution function analysis

Pair correlation function, RDF, demonstrates the probability of the presence of particles around one another. The correlation of the SO_2 molecules with all the zeolite atoms were investigated. Since the correlation between the SO_2 gas and O and Al ions of zeolite was weaker than the other Si and Na ions, they were not discussed in this paper. According to our findings, applying an external field intensified the correlation between the SO_2 gas and silica Y zeolite. Interestingly, the electric field was more effective in increasing the intensity of the RDF peak and the correlation of the SO_2-silica Y zeolite was in line with the results regarding SO_2/adsorbent affinity (Section 3.4).

Fig. 5b and c show the RDF of SO_2 with the Si and Na atoms of the NaY zeolite, respectively. As can be seen, the correlation of SO_2 with the Na atom of the zeolite was stronger compared to the Si atom of the zeolite. In this case, the adsorption distance in the Y zeolite was estimated at 4.5 Å while it was less than 4.0 Å in the case of the NaY zeolite. Furthermore, gas adsorption and its interaction with the adsorbent were stronger in the latter. As the adsorbate has a more robust interaction with the Na ions compared to the Si of NaY, it can be claimed that the appropriate site for gas accommodation to be near the metal ions gives the more basic features. As a result, presence of Na ion caused the higher adsorption capacity of the Si/Al= 3.0 zeolite (Table 1). In addition, the higher adsorption affinity of the Si/Al= 3.0 zeolite could be attributed to the presence of the Na ion in the Y zeolite.

3.4. Interaction energy of the SO_2/Zeolite

The interaction energy of SO_2 with the silica and Na cations of the NaY zeolite was computed in every target system in the presence and absence of the external electric and magnetic fields (Fig. 6). Our findings indicated that in all the studied systems, an energy well was observed at approximately 4.0 Å near the surface, which implied the surface adsorption of SO_2 on the zeolite that was slightly lower than 4.0 Å in the case of NaY. The difference between the bulk and minimum values of the PMF leads to a specific amount of adsorption energy. Some PMF plots experience a peak next to the energy well that shows the adsorption barrier energy of SO_2. In the present study, the developed adsorption capacity was dedicated to higher adsorption energy. The minimum, maximum, and bulk energies are marked by horizontal lines in Fig. 6.

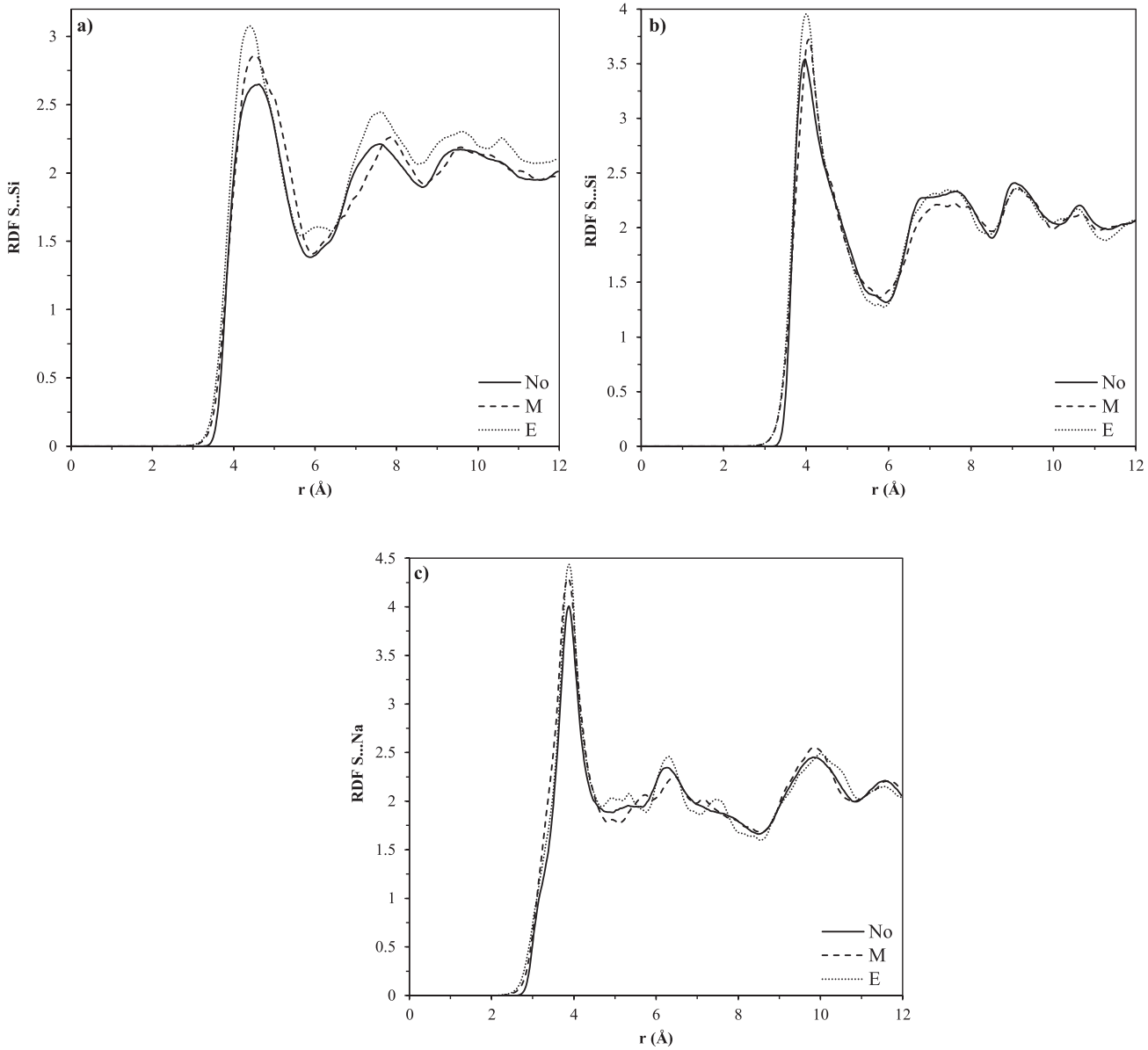

Fig. 5. RDF between S atom of gas and a) Si atom of silica Y zeolite, b) Si atom of NaY zeolite, and **c)** Na atom of NaY zeolite at 4.0 MPa and 300 K.

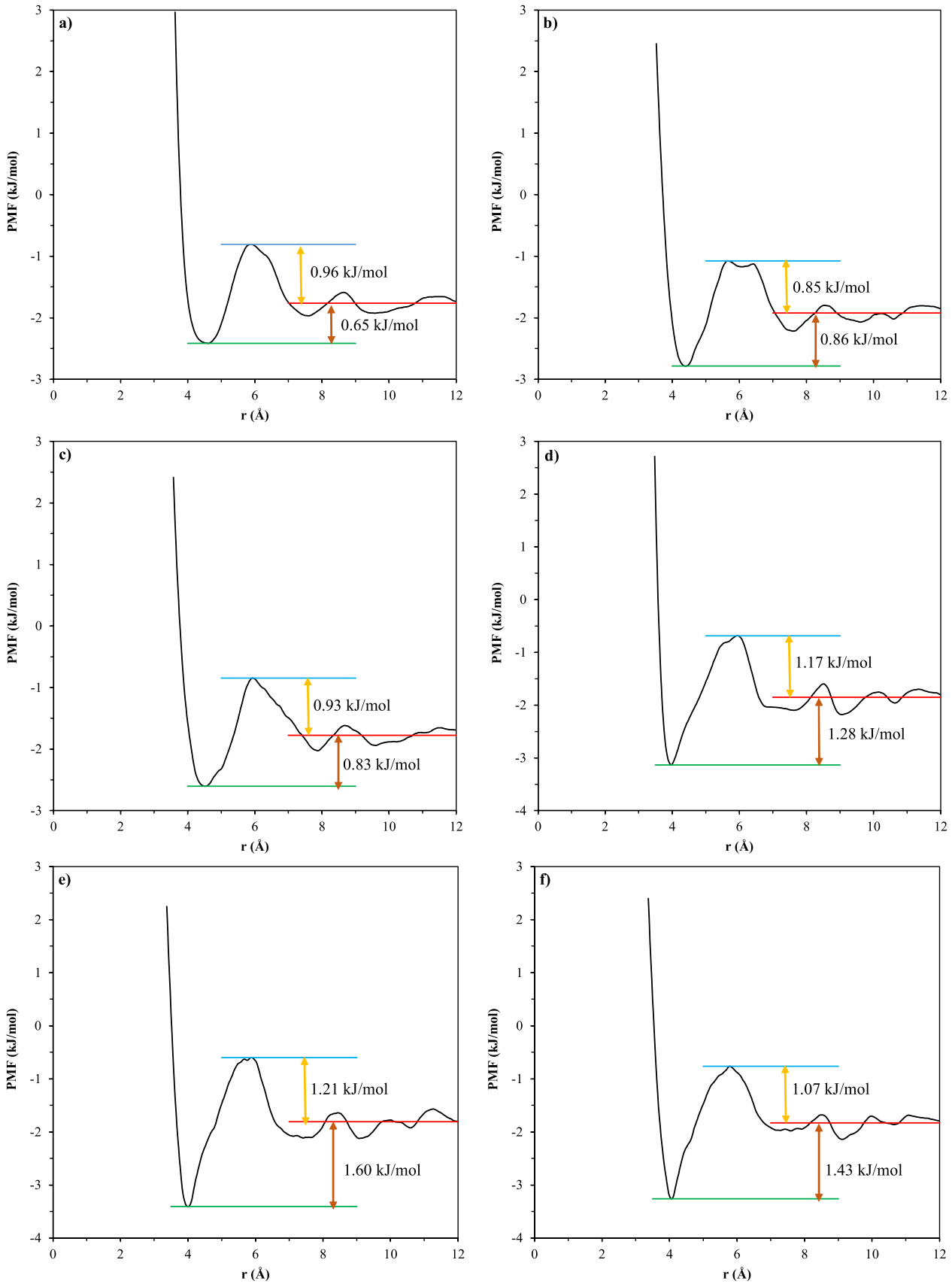

Fig. 6. Interaction energy of SO_2/zeolite in the case of silica Y; a) absence of external field, b) presence of electric field, c) presence of magnetic field; interaction energy between SO_2 and NaY zeolite d) absence of external field, e) presence of electric field, f) presence of magnetic field; interaction energy of SO_2/Na in NaY zeolite g) absence of external field, h) presence of electric field, and i) presence of magnetic field. Red line refers to PMF at $r \rightarrow \infty$.

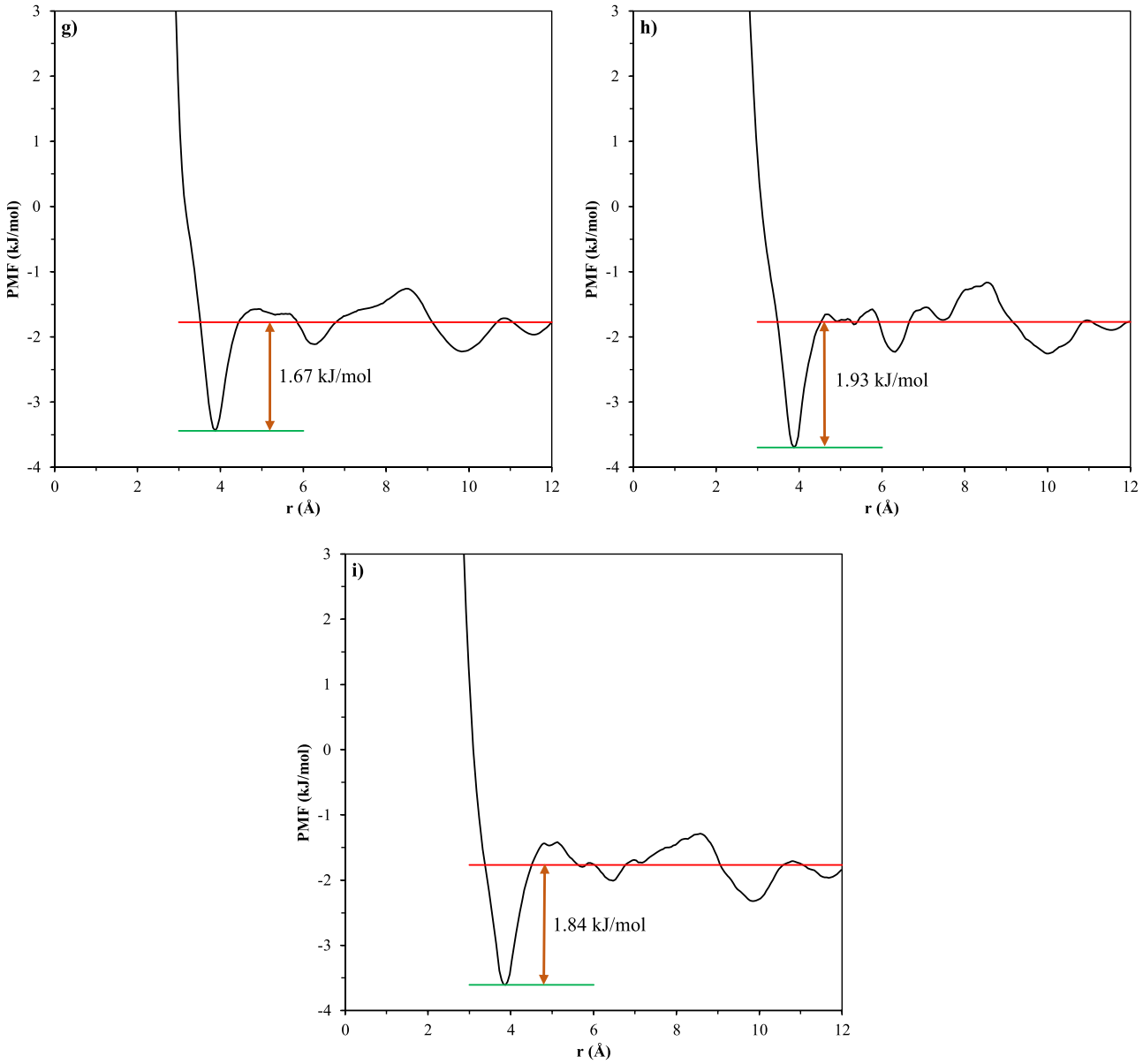

Fig. 6. (*continued*).

The noticeable point is that PMF values are obtained from RDF results according to Eq. 1 and it is smoothed at long distance. As a result, simulation results of $g(r)$ versus r can be extrapolated based on a waveform, damped sine, function to find adsorption energy, i.e., bulk energies. Applying the electric and magnetic fields in both zeolites reduced the energy barrier. Besides, the electric field enhanced the adsorption energy, thereby, increasing the SO_2-zeolite affinity. In some cases, the adsorption barrier energy is equal to zero (Fig. 6g-i) since there is no maximum next to the minimum point. Fig. 6g-i depict the interaction energy of SO_2 with the Na cations in the NaY zeolite. The adsorption of SO_2 to the cation of the NaY zeolite occurred spontaneously and no barrier energy was observed. Therefore, the presence of the cation increased the adsorption capacity and affinity in the NaY zeolite.

As can be seen in Fig. 6, the adsorption energy in NaY was 0.63 kJ/mol greater than the silica in the absence of the external field. Applying an external electric field could also increase the adsorption energy by 0.21 kJ/mol in SiO_2 and by 0.32 kJ/mol in NaY demonstrating the more significant effect of the electric field on NaY zeolite adsorption. Then again, the magnetic field intensified the adsorption energy in both adsorbents by 0.18 and 0.15 kJ/mol in the Y and NaY zeolites, respectively, while also weakening the energy value compared to the electric field by 0.03 and 0.17 kJ/mol. Therefore, it could be concluded that the external electric field had a significant effect on SO_2 adsorption. Furthermore, the barrier energy was not directly correlated with the adsorption energy and the effect of the external field although the greater barrier energy led to stiffer desorption.

3.5. Radial/Angle () distribution function analysis

The orientation of the SO_2 molecules was investigated to determine the motivation for the changes in the interaction energy of the SO_2/zeolite in the presence of the external electric and magnetic fields. Figs. 7 and 8 illustrate the variation of α_{SO_2} (defined in Fig. 2) inside the aimed Y zeolites. The distribution of α_{SO_2} in the silica Y zeolite obeyed a scattered regime for the non-treated system (Fig. 7a). Applying the electric field changed this scattered regime into the most concentrated distribution regime and the range of 110–150° was considered the most probable orientation angle to display the ordered SO_2 molecules and the

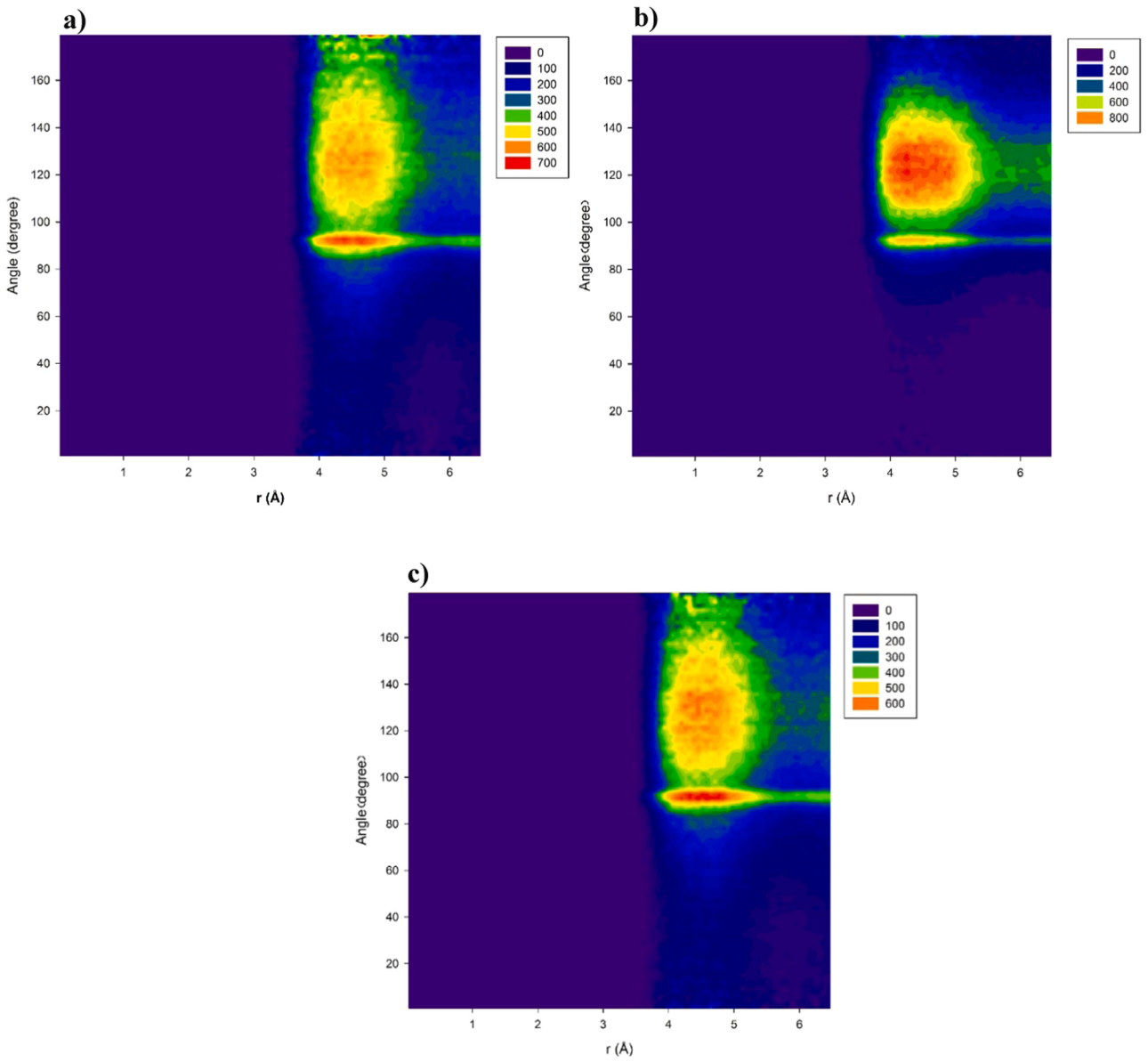

Fig. 7. RDF/ADF of silica Y zeolite; **a)** absence of external field, **b)** electric field in z-direction, and **c)** magnetic field in z-direction (RDF of SO_2/zeolite combined with ADF of α_{SO_2} at 4 MPa and 300 K).

gas adsorption capacity improvement by the Y zeolite (Fig. 7b). Alternatively, applying the magnetic field to this zeolite slightly increased the ordered orientation of the SO_2 molecules (Fig. 7c). As is depicted in Fig. 7, the angle distribution was more concentrated in the presence of an external field, with the most in the case of the electric field.

An erratic distribution was observed in the non-treated NaY zeolite and the external field (especially the electric field) changed the scattered regime to a concentrated ordered regime (Fig. 8). Since SO_2 is a polar gaseous molecule, applying the external electric field forced the dipoles to align towards the z-direction and the higher ordered orientation of the gas inside the zeolite led to more vacancies for the adsorption of the extra gas.

As can be seen in Figs. 7 and 8, the external magnetic and electric fields did not change the mean adsorption distance of the gas inside the zeolite.

3.6. *Effect of the Na cation on SO_2 adsorption*

In the present study, we investigated two Y zeolites with the Si/Al ratio of ∞ and 3.0 to compare the pair correlation of the adsorbed gas. In addition, the RDF between the gas and porous material was compared in the case of the untreated Y zeolites and gas adsorption in the absence of an external field was presented. Fig. 9 shows the comparison of the RDF of the gas inside the SiO_2 and NaY zeolites.

According to the obtained results, the correlation of the SO_2/zeolite increased in the presence of the Al particle in the structure and the SO_2 adsorption capacity in the Si/Al= 3.0 zeolite is considerably more extraordinary that was explained by two factors; the first factor was the increasing unbalanced charges inside the zeolite pores and the second one was enhancing the basicity of the zeolite framework by the Al^{3+} ion content due to the Na^{+} exchangeable cation [56]. This finding confirms that the interaction energy also increased based on the PMF results.

4. Conclusions

In this study, we simulated two Y zeolites (silica and NaY) in the presence and absence of electric and magnetic fields to assess the adsorption of SO_2 structurally and thermodynamically. According to the

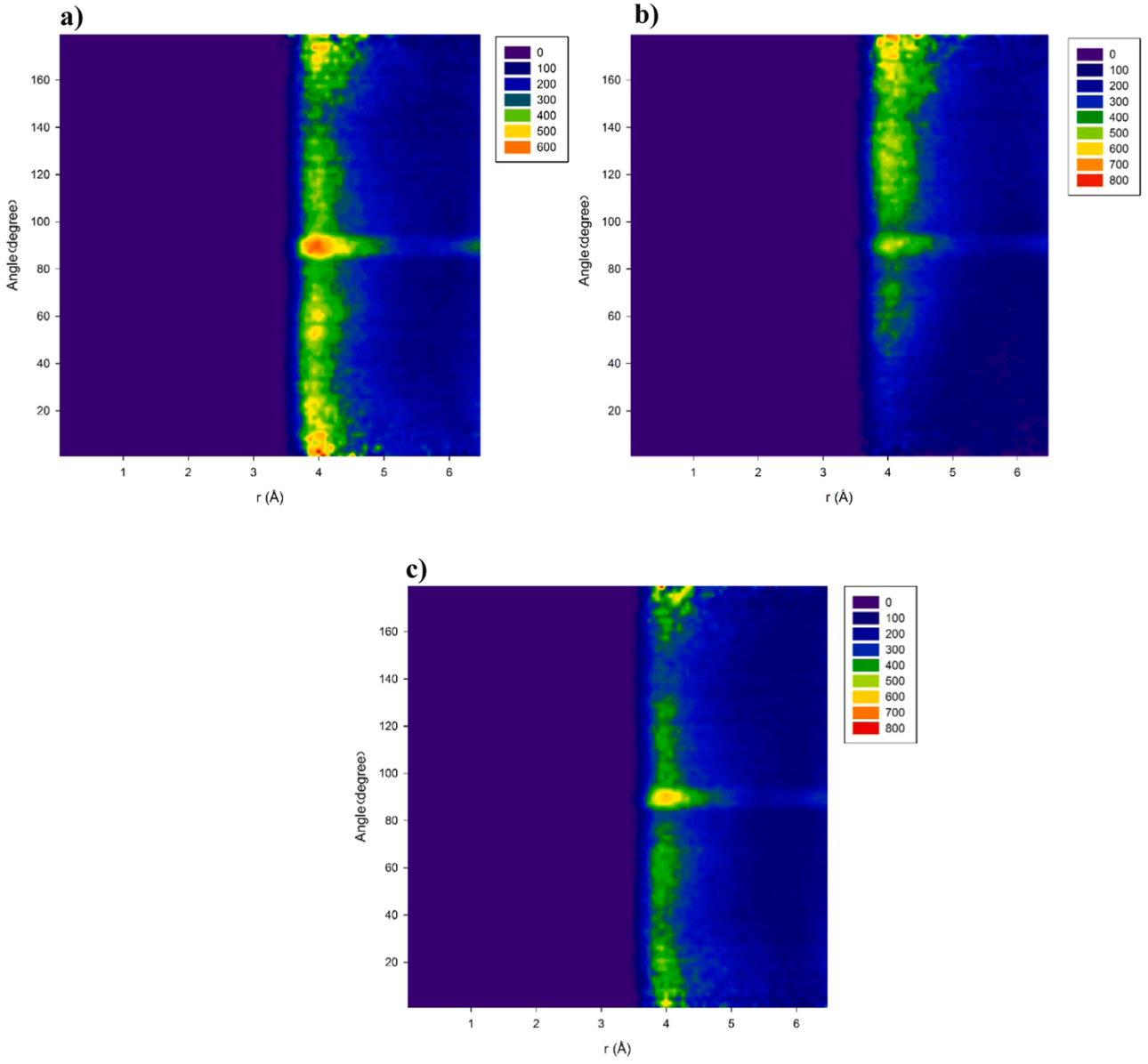

Fig. 8. RDF/ADF of NaY zeolite; a) absence of external field, b) electric field in z-direction, and c) magnetic field in z-direction (RDF of SO_2/zeolite combined with ADF of α_{SO_2} at 4 MPa and 300 K).

results, the SO_2-saturated adsorbent was regenerated completely in the simulation conditions through the effects of the external electric and magnetic fields. Furthermore, the presence of an electric/magnetic field improved the adsorption capacity of the material by approximately 12% at room temperature. Applying the electric field also increased the adsorption capacity at $P > 6.6$ MPa in the NaY zeolite. Moreover, the external field in both Y zeolites (silica Y and NaY) increased the sensitivity of adsorption, and the electric field was more effective compared to the magnetic field due to its higher adsorption capacity.

The Langmuir model indicated that the total saturated capacity was the highest in the presence of the electric field. However, magnetization slightly increased the saturated capacity; the potential of the mean force analysis showed that the interaction energy between the Y zeolite and SO_2 gas molecules caused a higher capacity of the electrically treated Y zeolite. In addition, the electric field could enhance the gas-Y zeolite interaction energy more significantly than the magnetic field. The interaction energy displayed the interaction of SO_2 with the zeolite, and SO_2 and Na ion interactions also increased in the presence of the external fields, especially the electric field. The radial distribution function of the SO_2-Y zeolite demonstrated that applying an external field in both Y zeolites improved the correlation, which was the main reason for the changes in the adsorption energy based on the PMF results.

As mentioned earlier, electric field plays a significant role in increasing the correlation of gas adsorbents. Combined distribution function points to the special ordering of the SO_2 gas inside the zeolite and was considered responsible for the enhanced gas capacity of the zeolite in the presence of the electric field. Due to the polar nature of SO_2 molecules, it tended to orient in the direction of the electric field. On the other hand, the investigation of the effects of the Si/Al ratio also indicated that by decreasing the Si/Al ratio of the Y zeolite, the adsorption saturation capacity increased as well, the gas and Y zeolite interaction energy enhanced, and the correlation of the SO_2-Y zeolite became more significant.

Our findings could broaden the horizons for increasing gas adsorption without changing the chemical structure of the adsorbent. In the case of a polar gaseous adsorbate, an electric field is expected to improve the gas capacity and its adsorption energy.

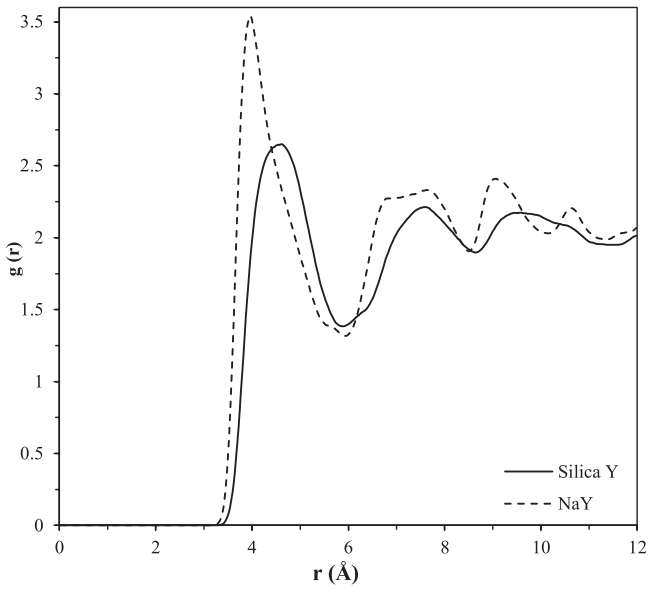

Fig. 9. RDF of SO_2 gas in untreated Y zeolites at 4 MPa and 300 K.

Declaration of Competing Interest

The authors declare that they have no known competing financial interests or personal relationships that could have appeared to influence the work reported in this paper.

Data Availability

The raw/processed data required to reproduce these findings cannot be shared presently due to legal and ethical matters. After acceptance, they will be made available to be downloaded from https://www.dropbox.com/home.

Acknowledgment

Hereby, we extend our gratitude to the HPC Center of Ferdowsi University of Mashhad for providing the facilities to perform part of the computations of this study. We would also like to show appreciation to Ferdowsi University of Mashhad (Grant No. 3/47414) for the financial support of this research project.

References

[1] S.E. Henkelis, D.L. Huber, D.J. Vogel, J.M. Rimsza, T.M. Nenoff, Magnetic tunability in RE-DOBDC MOFs via NO_x acid gas adsorption, ACS Appl. Mater. Interfaces 12 (17) (2020) 19504–19510.
[2] M. Mohammadi, M. Foroutan, Molecular investigation of SO_2 gas absorption by ionic liquids: Effects of anion type, J. Mol. Liq. 193 (2014) 60–68.
[3] Y. Zhu, J. Gao, Y. Li, F. Sun, J. Gao, S. Wu, Y. Qin, Preparation of activated carbons for SO_2 adsorption by CO_2 and steam activation, J. Taiwan Inst. Chem. Eng. 43 (1) (2012) 112–119.
[4] M.C.C. Ribeiro, Molecular dynamics simulation of liquid sulfur dioxide, J. Phys. Chem. B 110 (17) (2006) 8789–8797.
[5] H. Deng, H. Yi, X. Tang, H. Liu, X. Zhou, Interactive effect for simultaneous removal of SO_2, NO, and CO_2 in flue gas on ion exchanged zeolites. Ind. Eng. Chem. Res. 52 (20) (2013) 6778–6784.
[6] H. Yi, H. Deng, X. Tang, Q. Yu, X. Zhou, H. Liu, Adsorption equilibrium and kinetics for SO_2, NO, CO_2 on zeolites FAU and LTA, J. Hazard. Mater. 203–204 (2012) 111–117.
[7] D. Babu, D. Puthusseri, F. Kühl, S. Okeil, M. Bruns, M. Hampe, J. Schneider, SO_2 gas adsorption on carbon nanomaterials: a comparative study, Beilstein J. Nanotechnol. 9 (2018) 1782–1792.
[8] S. Gautam, V.K. Sharma, S. Mitra, S.L. Chaplot, R. Mukhopadhyay, Rotational dynamics of propylene in ZSM-5 zeolitic frameworks, Chem. Phys. Lett. 501 (4) (2011) 345–350.
[9] A. Buin, J. Ma, Y. Huang, S. Consta, Z. Hui, Conformational changes of trans-1,2-Dichlorocyclohexane adsorbed in zeolites studied by FT-raman spectroscopy and molecular QM/MM simulations, J. Phys. Chem. C. 116 (15) (2012) 8608–8618.
[10] M.H. Kowsari, S. Naderlou, Understanding the dynamics, self-diffusion, and microscopic structure of hydrogen inside the nanoporous Li-LSX zeolite, Microporous Mesoporous Mater. 240 (2017) 39–49.
[11] S. Dang, L. Zhao, J. Gao, C. Xu, Loading dependence of the adsorption mechanism of thiophene in FAU zeolite. Ind. Eng. Chem. Res. (45) (2016) 11801–11808, 2016 v.55 no.45.
[12] Y. Sun, S. Han, Diffusion of N_2, O_2, H_2S and SO_2 in MFI and 4A zeolites by molecular dynamics simulations, Mol. Simul. 41 (13) (2015) 1095–1109.
[13] I.-C. Marcu, I. Sȃndulescu, Study of sulfur dioxide adsorption on Y zeolite, J. Serb. Chem. Soc. 69 (7) (2004) 563–569.
[14] K.X. Lee, H. Wang, S. Karakalos, G. Tsilomelekis, J.A. Valla, Adsorptive desulfurization of 4,6-dimethyldibenzothiophene on bimetallic mesoporous Y zeolites: effects of Cu and Ce composition and configuration, Ind. Eng. Chem. Res. 58 (39) (2019) 18301–18312.
[15] D. He, P. Li, J. Hu, T. Wan, Kinetics of corrosive sulfur adsorption in transformer oil with Ag-Y, Ce-Y and Cu-Y zeolites, Adsorpt. Sci. Technol. 37 (5–6) (2019) 480–491.
[16] I. Khalil, H. Jabraoui, G. Maurin, S. Lebègue, M. Badawi, K. Thomas, F. Maugé, Selective capture of phenol from biofuel using protonated faujasite zeolites with different Si/Al ratios, J. Phys. Chem. C 122 (46) (2018).
[17] M.L.M.N. Cerutti, F.V. Hackbarth, D. Maass, S.S.X. Chiaro, R.R.C. Pinto, M.J. B. Cardoso, P.A. Arroyo, A.A. Ulson, de Souza, S.M.A.G.U. de Souza, Copper-exchanged Y zeolites for gasoline deep-desulfurization, Adsorption 25 (2019) 1595–1609.
[18] L.M. Rodríguez-Albelo, E. López-Maya, S. Hamad, A.R. Ruiz-Salvador, S. Calero, J. A.R. Navarro, Selective sulfur dioxide adsorption on crystal defect sites on an isoreticular metal organic framework series, Nat. Commun. 8 (1) (2017) 14457.
[19] N. Li, Y. Tian, J. Zhao, W. Zhan, J. Du, L. Kong, J. Zhang, W. Zuo, Ultrafast selective capture of phosphorus from sewage by 3D Fe_3O_4@ZnO via weak magnetic field enhanced adsorption, Chem. Eng. J. 341 (2018) 289–297.
[20] C. Zhao, J. Li, Y. He, J. Wang, W.Y. Wang, H. Kou, J. Wang, Effect of strong magnetic field on the microstructure and mechanical-magnetic properties of AlCoCrFeNi high-entropy alloy, J. Alloy. Compd. 820 (2020), 153407.
[21] F. Liu, F. Wang, G. Jia, The molecular dynamic simulation of dimethyl sulfoxide aqueous solution under the electric magnetic field, J. Mol. Liq. 225 (2017) 788–792.
[22] M. Razmkhah, M.T.H. Mosavian, F. Moosavi, A. Ahmadpour, CO_2 gas adsorption into graphene oxide framework: Effect of electric and magnetic field, Appl. Surf. Sci. 456 (2018) 318–327.
[23] Q. Sun, G. Qin, Y. Ma, W. Wang, P. Li, A. Du, Z. Li, Electric field controlled CO_2 capture and CO_2/N_2 separation on MoS_2 monolayers, Nanoscale 9 (1) (2017) 19–24.
[24] T. Zhang, H. Sun, F. Wang, W. Zhang, J. Ma, S. Tang, H. Gong, J. Zhang, Electric-field controlled capture or release of phosgene molecule on graphene-based materials: fFirst principles calculations, Appl. Surf. Sci. 427 (2018) 1019–1026.
[25] G.-q Qin, A.-j Du, Q. Sun, Charge- and Electric-Field-Controlled Switchable Carbon Dioxide Capture and Gas Separation on a C_2N Monolayer, Energy Technol. 6 (1) (2018) 205–212.
[26] M.D. Esrafili, *Electric field assisted activation of CO_2 over P-doped graphene: A DFT study*. J. Mol. Graph. Model. 90 (2019) 192–198.
[27] J. Ma, Y. Ma, F. Yu, X. Dai, Rotating magnetic field-assisted adsorption mechanism of pollutants on mechanically strong sodium alginate/graphene/l-cysteine beads in batch and fixed-bed column systems, Environ. Sci. Technol. 52 (23) (2018) 13925–13934.
[28] M.L. Costenoble, W.J. Mortier, J.B. Uytterhoeven, Location of cations in synthetic zeolites X and Y. Part 4.-Exchange limiting factors for Ca^{2+} in zeolite Y, Faraday Trans. 1: Phys. Chem. Condens. Phases 72 (0) (1976) 1877–1883.
[29] R.E. Fletcher, S. Ling, B. Slater, Violations of Löwenstein's rule in zeolites, Chem. Sci. 8 (11) (2017) 7483–7491.
[30] D.F. Plant, G. Maurin, H. Jobic, P.L. Llewellyn, Molecular dynamics simulation of the cation motion upon adsorption of CO_2 in faujasite zeolite systems, J. Phys. Chem. B 110 (29) (2006) 14372–14378.
[31] I. Déroche, G. Maurin, B.J. Borah, S. Yashonath, H. Jobic, Diffusion of pure CH_4 and its binary mixture with CO_2 in Faujasite NaY: a combination of neutron scattering experiments and molecular dynamics simulations, J. Phys. Chem. C 114 (11) (2010) 5027–5034.
[32] S.M. Auerbach, F. Jousse, D.P. Vercauteren, in: C.R.A. Catlow, B. R.A.v. Santen, Smit (Eds.), Chapter 3 - Dynamics of sorbed molecules in zeolites, in Computer Modelling of Microporous Materials, Academic Press, London, 2004, pp. 49–108.
[33] B.C. Bukowski, F.J. Keil, P.I. Ravikovitch, G. Sastre, R.Q. Snurr, M.-O. Coppens, Connecting theory and simulation with experiment for the study of diffusion in nanoporous solids, Adsorption (2021).
[34] Z. Tahraoui, H. Nouali, C. Marichal, P. Forler, J. Klein, T.J. Daou, Influence of the compensating cation nature on the water adsorption properties of zeolites, Molecules 25 (4) (2020) 944.
[35] I. Matito-Martos, A. Martin-Calvo, J.J. Gutiérrez-Sevillano, M. Haranczyk, M. Doblare, J.B. Parra, C.O. Ania, S. Calero, Zeolite screening for the separation of gas mixtures containing SO_2, CO_2 and CO, Phys. Chem. Chem. Phys. 16 (37) (2014) 19884–19893.
[36] J.B. Nicholas, A.J. Hopfinger, F.R. Trouw, L.E. Iton, Molecular modeling of zeolite structure. 2. Structure and dynamics of silica sodalite and silicate force field, J. Am. Chem. Soc. 113 (13) (1991) 4792–4800.
[37] J.C. Palmer, J.D. Moore, T.J. Roussel, J.K. Brennan, K.E. Gubbins, Adsorptive behavior of CO_2, CH_4 and their mixtures in carbon nanospace: a molecular simulation study, Phys. Chem. Chem. Phys. 13 (9) (2011) 3985–3996.

[38] Y. Kobayashi, S. Takami, M. Kubo, A. Miyamoto, Computational chemical study on separation of benzene and cyclohexane by a NaY zeolite membrane, Desalination 147 (1) (2002) 339–344.
[39] Z. Zhang, H. Liu, J. Zhu, B. Chen, H. Tian, Z. He, Molecular simulations of adsorption and diffusion behaviors of benzene molecules in NaY zeolite, Chin. J. Chem. Eng. 17 (2009) 618–624.
[40] W. Smith, T.R. Forester, DL_POLY_2.0: a general-purpose parallel molecular dynamics simulation package, J. Mol. Graph. 14 (3) (1996) 136–141.
[41] W. Smith, C.W. Yong, P.M. Rodger, DL_POLY: application to molecular simulation, Mol. Simul. 28 (5) (2002) 385–471.
[42] H. Zheng, L. Zhao, Q. Yang, S. Dang, Y. Wang, J. Gao, C. Xu, Insight into the adsorption mechanism of benzene in HY zeolites: the effect of loading, RSC Adv. 6 (41) (2016) 34175–34187.
[43] H. Zheng, L. Zhao, Q. Yang, J. Gao, B. Shen, C. Xu, Influence of framework protons on the adsorption sites of the benzene/HY system, Ind. Eng. Chem. Res. 53 (35) (2014) 13610–13617.
[44] M.A. Cuendet, W.Fv Gunsteren, On the calculation of velocity-dependent properties in molecular dynamics simulations using the leapfrog integration algorithm, J. Chem. Mol. 127 (18) (2007), 184102.
[45] E. Iskrenova-Tchoukova, A.G. Kalinichev, R.J. Kirkpatrick, Metal cation complexation with natural organic matter in aqueous solutions: molecular dynamics simulations and potentials of mean force, Langmuir: ACS J. Surf. Colloids 26 (20) (2010) 15909–15919.
[46] M. Razmkhah, M.T. Hamed Mosavian, F. Moosavi, Transport, thermodynamic, and structural properties of rare earth zirconia-based electrolytes by molecular dynamics simulation, Int. J. Energy Res. 40 (12) (2016) 1712–1723.
[47] M. Brehm, B. Kirchner, TRAVIS - a free analyzer and visualizer for monte carlo and molecular dynamics trajectories, J. Chem. Inf. Model. 51 (8) (2011) 2007–2023.
[48] M. Razmkhah, M.T. Hamed Mosavian, F. Moosavi, Structural analysis of an amino acid ionic liquid: Bulk and electrical double layer, J. Mol. Liq. 268 (2018) 506–516.
[49] R. Shi, Y. Wang, Ion-cage interpretation for the structural and dynamic changes of ionic liquids under an external electric field, J. Phys. Chem. B 117 (17) (2013) 5102–5112.
[50] M. Abbaspour, H. Akbarzadeh, S. Salemi, L. Bahmanipour, Phase transitions in nanostructured water confined in carbon nanotubes by external electric and magnetic fields: a molecular dynamics investigation, RSC Adv. 11 (18) (2021) 10532–10539.
[51] G.K. Rajahmundry, C. Garlapati, P.S. Kumar, R.S. Alwi, D.-V.N. Vo, Statistical analysis of adsorption isotherm models and its appropriate selection, Chemosphere 276 (2021), 130176.
[52] C.S. Dutcher, X. Ge, A.S. Wexler, S.L. Clegg, Statistical mechanics of multilayer sorption: extension of the Brunauer–Emmett–Teller (BET) and Guggenheim–Anderson–de Boer (GAB) adsorption isotherms, J. Phys. Chem. C 115 (33) (2011) 16474–16487.
[53] S. Rothenberg, Theoretical study of SO2 molecular properties, J. Chem. Phys. 53 (8) (1970) 3014–3019.
[54] C. Kachi-Terajima, T. Akatsuka, M.-a Kohbara, S. Takamizawa, Structural and magnetic study of N_2, NO, NO_2, and SO_2 adsorbed within a flexible single-crystal adsorbent of $[Rh_2(bza)_4(pyz)]_n$, Chem. – Asian J. 2 (1) (2007) 40–50.
[55] R. Yang, A. Jia, S. He, Q. Hu, M. Sun, T. Dong, Y. Hou, S. Zhou, Experimental investigation of water vapor adsorption isotherm on gas-producing Longmaxi shale: mathematical modeling and implication for water distribution in shale reservoirs, Chem. Eng. J. 406 (2021), 125982.
[56] A. Abdelrasoul, H. Zhang, C.-H. Cheng, H. Doan, Applications of molecular simulations for separation and adsorption in zeolites, Microporous Mesoporous Mater. 242 (2017) 294–348.